Guided ion beam measurement of the product branching ratios for the ion-molecule reaction $N^+ + O_2$ as a function of collision energy

Robert D. Guettler, Glenn C. Jones, Jr., Lynmarie A. Posey,[a] Nicholas J. Kirchner,[b] Beat A. Keller,[c] and Richard N. Zare[d]
Department of Chemistry, Stanford University, Stanford, California 94305

(Received 21 March 1994; accepted 13 May 1994)

A quadrupole-octopole-quadrupole mass spectrometer has been constructed for comparing ion-molecule reaction product intensities as both the internal excitation and the kinetic energy of the reactant ion are varied. Such comparisons require an ion beam with a known kinetic energy distribution and, most importantly, they require product intensity measurements made without significant bias in detection of the different product channels. To assess the characteristics of our instrument, we have studied the ion-molecule reaction $N^+ + O_2$ that is known to yield three different product channels: $N + O_2^+$, $NO^+ + O$, and $NO + O^+$. Ion beam trajectory simulations combined with experimental measurements show that the spread in the kinetic energy of the reagent ions has a fixed value in the range of 0.6 to 1.1 eV full width at half maximum in the center of mass (c.m.). Relative cross sections for the three different product channels are reported as a function of c.m. collision energy. A comparison of the observed product branching ratios with those determined previously by other workers shows that no serious product discrimination occurs over the collision energy range of 1.5 to 10.0 eV c.m. Discrepancies in the product branching ratios below 1.5 eV c.m. are believed to be caused by the overall collision energy uncertainty that results from both the ion beam kinetic energy spread and the thermal motion of the O_2 reactant.

I. INTRODUCTION

We have recently constructed a quadrupole-octopole-quadrupole mass spectrometer to carry out state-selected studies on ion-molecule reactions. The primary purpose of the instrument is to measure product ion intensities as both the vibrational excitation and kinetic energy of the reactant ions are changed. In these studies, the reactant ions are to be vibrationally state selected and mass selected before reaction with a thermal, neutral gas at a fixed collision energy [1–10 eV center of mass (c.m.)]. Product and reactant ion intensities should be monitored free from discrimination caused by their mass or relative scattering. From these intensities, the product branching ratios and relative cross sections of the reaction system are determined as the vibrational state and kinetic energy of the reactant ion are varied, which will demonstrate the role that vibrational motion plays in determining the reaction outcome. These observations may also provide insight into the nature of the reactive interaction leading to product formation. An example of such a state-selected study carried out with this instrument is presented in a companion paper that investigates the ion-molecule reaction of $NH_3^+(\nu_2) + ND_3$.[1]

Several key experimental questions become apparent when considering the studies outlined: (1) Can state-selected ions be generated with sufficient flux and reacted with state selectivity intact? (2) Can the reactant ion kinetic energy be accurately controlled and have a narrow enough spread to yield meaningful collision energies? (3) Most importantly, can product intensities be measured without significant channel-dependent discrimination? Answers to these questions must precede rigorous interpretation of any observed reaction system properties. The affirmative answer to the first question is demonstrated in the following paper on the state-selected ion-molecule reaction of $NH_3^+ + ND_3$.[1] The answers to the second and third questions concerning instrument performance are the focus of this report.

Because the collision energy is set by the easily controlled kinetic energy of the reactant ion, the second question concerning the collision energy is answered by examining the energy characteristics of the reactant ion beam. These characteristics are determined and discussed in Sec. II. A comprehensive check on the many factors that may contribute to channel-dependent discrimination is to measure with this instrument a reaction having a well-characterized product branching ratio. The amount of channel-dependent discrimination present in this instrument can be gauged by comparing the measured branching ratios to those obtained previously and using the observed discrepancy to constrain the interpretation of measurements made with this instrument.

The system selected to test for product-dependent discrimination should meet several criteria. The first two criteria concern the reaction system itself. (1) The desired system must have multiple product channels for which the branching ratios have been measured over the collision energy range

[a]Current address: Department of Chemistry, Vanderbilt University, Nashville, Tennessee 37235.
[b]Current address: Massively Parallel Instruments, Inc., 2030 Fortune Drive, Suite A, San Jose, California 95131.
[c]Current address: Swiss Federal Laboratories for Materials Testing and Research, CH-8600, Switzerland.
[d]Author to whom all correspondence should be directed. E-mail: rnz@chemistry.Stanford.EDU

 0021-9606/94/101(5)/3763/9/$6.00

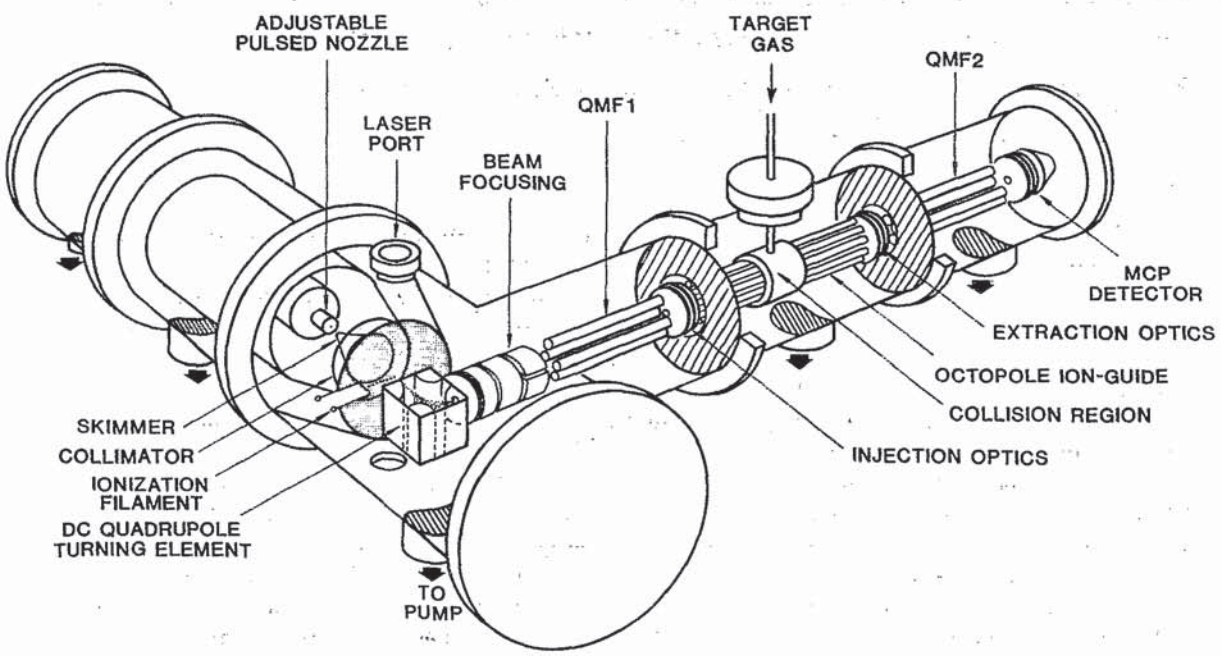

FIG. 1. Schematic illustration of the quadrupole-octopole-quadrupole mass spectrometer employed to study ion-molecule reactions with electron impact ionization or state-selective preparation of the reagent ions by resonance-enhanced multiphoton ionization. (QMF is the quadrupole mass filter; MCP is the microchannel plate.)

investigated with this instrument (0.5–10.0 eV c.m.). (2) It should have product masses near those of the principal state-selected system of interest, $NH_3^+ + ND_3$ (17–22 a.m.u.). The final two criteria for the test system concern the methods used in the measurements. (3) The reactant ion must be generated in a way that makes comparison to the state-selected photoionization studies relevant. Because ion state selection is accomplished by (2+1) resonance-enhanced multiphoton ionization, we desired a test system for which photoionization could be used to generate ions. Unfortunately, the sparseness of reaction systems amenable to photoionization that are well characterized at superthermal collision energies has forced us instead to adopt the more conventional electron impact ionization scheme for these characterization studies. Yet even with electron impact ionization, the number of systems meeting the previous two criteria is small. (4) Because our quadrupole-octopole-quadrupole instrument relies heavily upon the use of radio-frequency (rf) devices, a comparison reaction system is sought that has been studied with techniques that do not employ guided ion beams. In this instrument, the rf octopole ion guide is used to direct the reactant ions to the collision region and to guide all the product ions, regardless of their reactive scattering and mass, to the second quadrupole for subsequent mass analysis and detection. As will be seen later, these rf devices have a significant role in the answers to the questions concerning instrumental performance addressed herein. Therefore, this final criterion will avoid any chance of duplication of discrimination factors resulting from experimental similarities. Preferably, the results for the test reaction system will have been obtained by several different methods so that any method-dependent discrimination is avoided.

The system that appears to come closest to meeting all of these criteria is the $N^+ + O_2$ ion-molecule system. The three primary product channels of the $N^+ + O_2$ system are

$$N^+ + O_2 \rightarrow N + O_2^+ \tag{1a}$$

$$\rightarrow NO^+ + O \tag{1b}$$

$$\rightarrow NO + O^+. \tag{1c}$$

The reaction was studied by several techniques over a wide range of collision energies.[2–6] The highest collision energies have been measured with a crossed-beam experiment[2] (1.5–40 eV c.m.). Selected-ion flow-drift tube measurements[3] have been made in the collision energy range 0.06–1.8 eV c.m., between the several thermal measurements[4–6] and the lowest energies of the crossed-beam measurements. The two superthermal data sets completely span the range of collision energies to be investigated with our quadrupole-octopole-quadrupole instrument and, hence, form the basis of the present characterization study.

II. EXPERIMENT

Figure 1 presents a schematic diagram of our quadrupole-octopole-quadrupole instrument. Ionization occurs in a pulsed molecular beam by electron impact ionization or photoionization. For the present study of the $N^+ + O_2$ reaction system, the N^+ ions were formed exclusively by electron impact. An example of photoionization work with

this instrument is presented in the following paper on the state-selected ion-molecule reactions of $NH_3^+ + ND_3$.[1] The reactant ions are extracted from the molecular beam and passed through a quadrupole mass filter to ensure that only ions of the desired mass enter the subsequent reaction region. The ions are accelerated to the desired kinetic energy as they enter the octopole ion guide. The ion guide passes through the collision cell, thus serving to transport the reactant ions to the collision cell, which contains the neutral reactant molecule, and to guide the product ions and remaining reactant ions to the second quadrupole mass filter. This second mass filter selects the ion mass to be detected, and from the product and reactant intensities, product branching ratios and relative cross sections are determined. A more detailed discussion of the instrument is provided in Secs. II A–II C, followed by a characterization of the reactant ion beam kinetic energy and a discussion of the overall collision energy spread.

A. Ion beam source

The species to be ionized is introduced into the instrument as a neat or seeded molecular beam. To generate N^+, N_2 (Matheson, 99.999%) neat or 10% in He (Liquid Carbonic, 99.995%) was expanded from a pulsed valve (General Valve #9-376-900, orifice diameter 0.15 mm). No significant difference in the N^+ intensity or energy characteristics was observed when seeding in helium. The position of the pulsed valve is externally adjustable in three dimensions. The molecular beam is formed by skimming (Beam Dynamics, Inc., 0.49 mm diameter orifice) and collimating (2 mm diameter orifice) the pulsed valve output. The skimmer is located 1–5 mm from the valve, and the collimator is ~5 cm from the skimmer tip. In this study, the pulsed valve was operated at frequencies of 10–30 Hz and stagnation pressures between 20 and 40 psi. The width of the valve pulse was adjusted so that the pressure in the vacuum chamber containing the valve did not exceed 5×10^{-6} Torr. Pulse widths were typically 300 μs full width at half maximum (FWHM). The pressure in the differential pumping chamber between the skimmer and the collimator was typically 6×10^{-7} Torr. With neutral reagent gas flowing into the collision cell in the adjacent chamber, the ionization chamber pressure was 3×10^{-7} Torr, slightly higher than the base pressure of 2×10^{-7} Torr.

Electron impact ionization occurs at a distance ~0.5 cm after the molecular beam collimating plate in a field-free region maintained at a controlled potential. The electron source is a tungsten filament that is voltage biased to accelerate the thermionic electrons to the desired kinetic energy in the field-free ionization region. The electrons pass through a triple layer of mesh as they enter the ionization region and cross the molecular beam at right angles. For this work, N^+ was generated by direct electron impact dissociative ionization of N_2 using electron energies of ~50 eV and filament emission currents of ~0.25 mA. After ionization, the ions continue to travel with the molecular beam pulse for ~1.5 cm beyond the electron impact point, where they enter a dc quadrupole turning element.[7–9]

The turning element extracts the ions from the molecular beam, directing them down the ion beam axis at right angles to the molecular beam axis. The ions travel through ~8 cm of electrostatic focusing optics (asymmetric lenses) before entering the first quadrupole mass filter (Finnigan, rod diameter 6.25 mm, length ~14 cm). The mass filter is driven by a Finnigan Model 3200-1 spectrometer control module (frequency 1.850 MHz, ion kinetic energy ~6 eV). One of the lenses leading to the first quadrupole is a split lens element that is pulsed to deflect the background N^+ ions formed by the continuous electron impact current. This lens is set to transmit ions throughout the duration of the molecular beam pulse. The non-rf ion optics voltages in the instrument are set by optimizing the N^+ signal intensity reaching the detector. Chopping with the split lens ensures that it is the transmission of N^+ originating from the molecular beam that is optimized.

The interface between the first quadrupole and the octopole ion guide is a set of three thin lenses (0.64 mm thick, 1.1 mm spacing, 3.2 mm aperture). The final lens has a 1.9 mm extension that penetrates into the octopole ion guide to help minimize fringing field effects from the ends of the octopole rods. These injection lenses prepare the strongly divergent ion beam exiting the quadrupole for entry into the octopole. Their electrostatic focusing acts to collimate some of the less divergent ions exiting the quadrupole, and these lenses also act as physical collimators, their apertures clipping the strongly divergent ions that have acquired significant radial velocity components within the quadrupole mass filter. These two purposes share a common objective: to produce an ion beam that upon injection into the octopole ion guide is well collimated, with radial velocity components (perpendicular to the ion beam axis) significantly less than the axial velocity components (parallel to the ion beam axis). This objective is an integral part of the ion beam energy characteristics discussed later.

B. Collision region

The collimated ion beam enters the octopole ion guide (0.318 cm rod diameter, 0.476 cm inscribed radius, 27.9 cm long), which has a dc voltage set to provide the ions with the desired kinetic energy. Ervin[10] has shown that the best approximation to a hyperbolic multipole that can be achieved with cylindrical rods corresponds to a geometry in which the ratio of the rod radius to inscribed radius, a/r_0, is 0.37; for our octopole $a/r_0=0.33$. The octopole and driving electronics are partially homebuilt, using an ICOM Transceiver (IC-735) as the rf sine-wave source and amplifier, that feeds an Extrel High Q-Head (Model 10) rf step-up transformer. Resonance matching between the source and the transformer was accomplished by an antenna matching device (MFJ, Model MFJ-949C). The rf potential supplied to the ion guide was typically 370 V peak rf voltage at a frequency of 4.70 MHz. The octopole ion guide functions as an "ion pipe," allowing nearly all the product ions to be transported from their formation point to the second quadrupole mass filter even when the product ions scattered from the reactive collision have significant off-axis velocity components.

Previous work in this laboratory[11–15] used a static collision cell to carry out ion-molecule reaction studies and, hence, was susceptible to variations in product collection ef-

ficiencies that resulted from differences in product recoil energetics. The octopole ion-guide eliminates this discrimination in product ion detection, making it possible to compare directly different product channels and determine product branching ratios and relative reaction cross sections. The octopole ion guide offers several advantages over the rf-only quadrupole commonly used in analytical chemistry. These advantages can be appreciated by examining the expression for the time-averaged effective trapping potential, U_{eff}, in a hyperbolic multipole as a function of the radial distance r for a particle of mass m and charge q (Refs. 10 and 16)

$$U_{\text{eff}}(r)=\frac{n^2q^2V_0^2}{4m\omega^2r_0^2}\left(\frac{r}{r_0}\right)^{2n-2}+U_s, \tag{2}$$

where $2n$ is the number of poles, $\pm V_0$ is the peak rf voltage of adjacent rods, $\omega/2\pi$ is the frequency, r_0 is the inscribed radius, and U_s is the dc potential on the octopole, which determines the beam energy. For a given inscribed radius, rf amplitude, frequency, and ion mass, the trapping potential of an octopole ion-guide, which has an r^6 dependence, is much deeper than that of a quadrupole, which has an r^2 dependence. In addition, the trapping potential of an octopole ion guide more closely approximates a square well, resulting in less perturbation of the ions as they move off axis. Further details concerning the operation of rf ion guides are given elsewhere.[10,17,18]

The collision cell is located ~16.5 cm beyond the octopole ion-guide entrance. The walls of the collision cell are formed by two ring electrodes that connect the sets of octopole rods. Gas is introduced in the 1.6 mm gap between the two electrodes, effusing between the ring electrodes and into the center of the ion guide as a thermalized gas. The collision cell walls do not penetrate into the circumscribed radius of the octopole rods, leaving large holes (0.79 cm radius) at the entrance and exit to the collision region. This open geometry is the most significant problem in making meaningful assignments to the collision region pressure and path length. The product and unreacted reagent ions travel the remaining length of the octopole heading toward the second quadrupole mass filter.

Gas flow to the collision cell is controlled by regulating the pressure backing a leak valve (Varian, Model 951-5100) which leads to the collision cell. The pressure is monitored on each side of the leak valve (14.8–15.1 psi and 0.9–1.1 Torr, respectively) and in the vacuum chamber containing the collision cell ($1.0–1.2\times10^{-6}$ Torr, base pressure: 1×10^{-7} Torr). The pressure between the leak valve and the vacuum chamber is measured with a convectron pressure gauge (Granville-Phillips Series 275), and the pressure in the vacuum chamber is measured with an uncalibrated Bayard-Alpert-type ion gauge (Granville-Phillips Series 307). The convectron gauge leading to the vacuum chamber proved the more sensitive measure of gas flow.

Near single-collision conditions were assured by monitoring the secondary products in the $NH_3^+ + ND_3$ reaction system, as described in the following article.[1] The $N^+ + O_2$ system has no secondary products distinguishable based on mass, whereas the $NH_3^+ + ND_3$ system has an easily observed secondary product that is formed by reaction of the charge transfer product (ND_3^+) with another ND_3. The ND_3^+ charge transfer product is expected to be moving with considerably less velocity than the incident NH_3^+ reactant and, by comparison to the analogous NH_3 system,[19–21] these slower secondary collisions are expected to yield predominantly ND_4^+. As with the NH_3 system, the cross section for ND_4^+ formation is expected to be nearly collisional,[21,22] and is therefore taken to be a direct indication of the extent to which secondary reactions are occurring. The pressure conditions of the collision cell obtained with $NH_3^+ + ND_3$ were also used for the $N^+ + O_2$ study. No correction was made for the differing detection sensitivities of the pressure measuring devices to NH_3 and O_2. However, when the collision cell pressure was increased to bring the collision chamber pressure to 3×10^{-6} Torr, a factor of 3 change, no change in product branching ratio was observed.

C. Detection and data collection

The ions are directed from the octopole ion-guide into the second quadrupole mass filter (Extrel, pole diameter 15.9 mm, length 22 cm) by a set of three lenses (6.3 mm aperture, 1.6 mm spacing). The potential difference between the dc offset of the second quadrupole and the octopole was kept constant at approximately −15 V. The second mass filter was driven by commercial electronics manufactured by Extrel (Model 111-0 Power supply, ~3.2 MHz frequency; 525 V_{rf} peak rf voltage at $m/e=17$). The objective of this quadrupole-octopole interface is the opposite of the injection interface at the octopole entrance. Ideally, *all* ions are to be transported from the ion guide to the quadrupole mass filter; the interface optics should obstruct no ions. This goal is aided by making the lens apertures larger than the octopole effective potential radius (effective potential, ~1 V at 2 mm, lens aperture radius, ~3 mm). To ensure that the quadrupole mass filter is operating with as high a detection sensitivity as possible, the mass resolution was decreased to yield nearly baseline resolution for peaks separated by one mass-to-charge ratio.

Following the mass filter is a set of two lenses (12.7 mm aperture, 1.6 mm spacing) that direct the ions to the detector and act to isolate the detector from the oscillating rf fields of the quadrupole mass filter. The ions are accelerated across a ~1.5 cm, −400−−2000 V voltage gradient that brings them to the detector. The detector is a chevron microchannel plate assembly (Galileo Electro-Optics FTD-2003) that is contained in a vacuum chamber at an operating pressure of 3×10^{-7} Torr, with gas being supplied to the adjacent collision cell. Typical ion flight times for the entire instrument, from ionization to detection, are 110 μs at a collision energy of 1.85 eV lab, corresponding to a total traversed distance of ~80 cm.

The output from the microchannel plates is fed to a dual-output 10× preamplifier (LeCroy 612A). The two output channels are used to drive two detection schemes, ion counting and analog detection. This dual data treatment provides the ability to detect a wide range of signal intensities. In the present $N^+ + O_2$ study, signal rates were never sufficient to require the use of the analog detection scheme; all signal intensities were determined by single ion counting. In the

counting detection scheme, the output of the preamplifier was fed into a 150 MHz discriminator (LeCroy 4608C). A multichannel scalar (MCS) (homebuilt, with DSP QS-450 100 MHz quad scalar front end) receives the discriminator output and stores the summed time-of-flight (TOF) profile. The scalar is read out by a digital computer (486–33 MHz, IBM compatible) via a CAMAC Crate (Kinetics Systems, Model 1502). The computer sums the TOF profiles for the various mass channels and controls the second quadrupole mass setting. A typical data collection cycle involves (1) setting the second quadrupole to the desired mass with the computer; (2) letting the scalar sum for the desired number of molecular beam pulses (50–400 pulses); (3) reading out the MCS with the computer and adding this data to the previously stored TOF data; and (4) repeating this sequence for the reactant and each of the product mass channels, which results in a summed TOF profile for each mass. This data collection cycle is repeated for typically 2–4 h (30–40 cycles) to generate a reactant and product set of TOF data for a given collision energy.

The TOF profiles are integrated, and the resulting product and reactant intensities are used to generate branching ratios and relative cross sections. The branching ratios are the fraction of summed product intensity in a particular product channel, and the relative cross sections are simply the ratio of the particular product intensity to the reactant intensity. Reactant ion intensities are not corrected for product formation because the fraction reacted is approximately 1×10^{-4}. With typical reactant intensities ranging from 5–15 ions/molecular beam pulse, the largest product intensities (NO^+) were typically one ion for every 20–30 molecular beam pulses. The weakest product channel intensity (O^+), one ion per 250 molecular beam pulses, was sufficiently small to require a detector dark current correction. An estimate of the dark current was obtained by monitoring blank mass channels ($m/e=23,28,29$) simultaneously collected with the reaction data. Typical dark currents were one count in 350–400 molecular beam pulses. Each experimental ion intensity was corrected by subtracting the dark current measured with that data set.

D. Ion beam kinetic energy characterization

This section is rather technical and more details are available elsewhere.[23] The collision energy of the reaction system is controlled by varying the kinetic energy of the reactant ion in the collision region, which is determined in large part by the potential difference between the ionization region and the collision region. The exact kinetic energy of the ion in the collision region will differ from this potential difference by an additional energy offset and it will have some characteristic spread. Determining these additional ion beam characteristics is complicated by the nature of this instrument, primarily, its heavy reliance on rf devices to mass select and then guide the ion beam to the collision region. Several approaches have been undertaken to estimate the energy offset and spread that occur in conjunction with the experimentally controlled potential difference kinetic energy.

The initial contribution to the ion beam kinetic energy is from the molecular beam source, which provides the ions with their initial velocity and spread. Because the molecular beam temperature is estimated to be tens of Kelvin, this initial contribution to the ion beam is small with respect to the collision energies investigated in the present work and small with respect to the measured energy spreads (see the following). Hence, the ion beam energy spread results primarily from subsequent instrumental effects.

When the reactant ion collides with the neutral reagent in the cylindrical octopole ion guide, it will have an axial and radial velocity component. The characteristics of the axial velocity component are estimated from two experimental techniques, a retarding potential analysis and a time-of-flight analysis. Each method yields the axial kinetic energy offset and spread of the ion beam. The radial velocity component is more difficult to assess. Although experimental methods exist for measuring the radial kinetic energy within an rf ion guide,[24] the investment necessary to obtain meaningful measurements is substantial. We have chosen instead to rely upon trajectory simulations to estimate the radial energy characteristics of the reactant ions inside the ion guide. The combined axial and radial information allows rough estimates to be made of the reactant ion kinetic energy magnitude and spread within the ion guide, from which the reaction collision energy magnitude and spread can be determined.

As the reactant ion beam enters the collision cell, it has interacted with two rf devices, the first quadrupole mass filter and the octopole ion guide. We have attempted with the optics design at the octopole entrance to prevent the radially energized ions of the quadrupole mass filter from entering the octopole ion guide, ensuring that the radial kinetic energy component of ions entering the octopole is an insignificant amount of the total ion kinetic energy. The trajectory calculations used to check the performance of this design were done with the commercial software program MacSimion.[25]

The two-dimensional nature of the trajectory software and the differing symmetries of the ion optics along the ion beam path forced the simulations to be carried out in three stages: the first quadrupole mass filter, the octopole injection optics, and the octopole ion guide. In our apparatus (Fig. 1), the elements that direct the ion beam to the first quadrupole mass filter are static ion optics. Their contribution to the radial velocity components is expected to be small relative to those introduced in the quadrupole mass filter, which experimentally[26] and theoretically[27–29] has been shown to yield potentially divergent ion beams. Therefore, our energetic analysis began with the first quadrupole mass filter.

With the known geometry and the fixed operating parameters of the first quadrupole, the dc and rf amplitudes were found by varying both values until stable trajectories for mass 17 ($^{14}NH_3^+$) (Ref. 1) were obtained at a "resolution" of roughly 17. From the time-averaged radial position and energetic profiles of these trajectories, reasonable ranges were chosen for the initial conditions of the octopole injection optics trajectories.

The most challenging aspect of modeling the octopole injection optics was to include to some degree the interaction between the rf quadrupole fields and the static injection lens fields. The true nature of the quadrupole-octopole interface

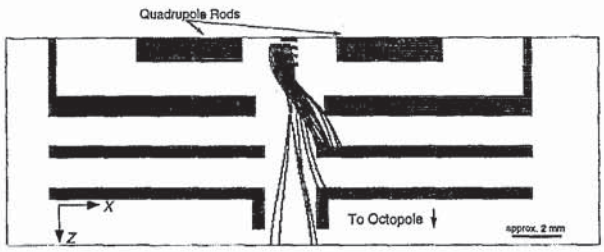

FIG. 2. Octopole injection optics and sample trajectories from MacSimion showing ion trajectories exiting the first quadrupole, passing through the injection optics, and entering the octopole. Initial conditions: 0–1.5 mm quadrupole radius; 1 eV radial energy; 5.9 eV axial energy. Electrodes at the top center between the quadrupole rods are those added to approximate quadrupole potential well (see text).

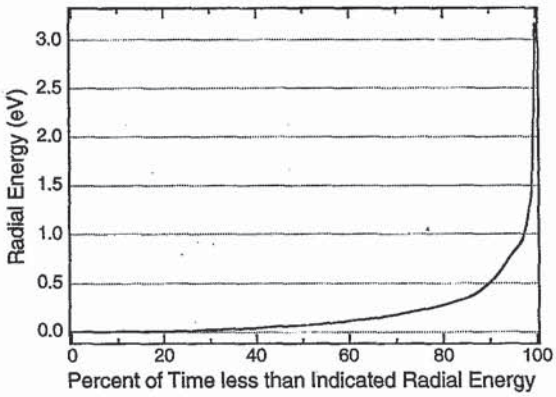

FIG. 3. Radial energy plotted as a function of percentage of total time steps below that energy. Percents are based on time steps summed over a complete set of octopole trajectories.

cannot be approximated without in some way accounting for the interaction of the static extraction lenses with the time-varying quadrupole potential. To accomplish this task within the constraints of the simulation software, approximately 1 mm of a quadrupole rod pair were included in the x-z plane of the injection optics electrode geometry (Fig. 2). A pseudo-potential well was created between the two rods by locking some of the center potential array points at a voltage that mimics the nature of the quadrupole potential well while leaving the protrusion and nature of the static lensing potentials as unchanged as possible. This limited and artificial inclusion of the quadrupole mass filter in this work was sufficient to demonstrate the large, and thereby crucial, difference the presence of the rf field had on the resulting injection lens trajectories. The octopole field was not included in the injection optics simulation because it has a much flatter and broader potential well than that of the quadrupole and therefore does not interact as significantly with the lensing.

The three-lens injection optic yields a highly skimmed and collimated ion beam that enters the octopole. When trajectories were run at the experimental voltages for these optics, most of the ions that exit the quadrupole struck aperture walls (Fig. 2). Those that passed through the injection lenses were highly collimated and had a small degree of divergence, less than 0.1 eV lab radial kinetic energy. This result is consistent with the experimentally observed intensity of the photoionized reagent beam in our $NH_3^+ + ND_3$ study.[1] Typical NH_3^+ reactant intensities were 100–150 ions per laser shot, although approximately 10^5–10^6 ions are produced in the ionization volume of the laser. When the quadrupole potential well was not included in the simulation, nearly all the ions were transported through the injection optics, which results in the incorrect picture of an intense but highly divergent ion beam entering the octopole.

The completed trajectories from the injection optics provide the initial radial positions and energies for the octopole trajectories. These initial radial positions and energies were oriented at each of three angular coordinates, $\theta=0$, $\pi/8$, and $\pi/4$. The results at these angles were weighted by 1:2:1, respectively, since the $\pi/8$ and $3\pi/8$ angles are equivalent. The trajectories were run for 7 μs, a compromise between data file size and the actual time required to arrive at the collision region. The energetics of these trajectories were analyzed by combining all of their time steps into a radial kinetic energy histogram and calculating a time-averaged radial energy distribution.

As expected, the average energy and the energy spread showed a strong dependence on the radial injection position, which indicates the lasting impact of the interaction between the initial trajectory steps and the sharply rising potential "wall" of the rf potential well. We find, however, that the fraction of trajectory steps at anomalous kinetic energies is small relative to the total number of time steps. This behavior is apparent from an energy distribution histogram and from the secondary analysis of this histogram presented in Fig. 3. Figure 3 shows the fraction of total trajectory time steps that fall below a given energy level. From this plot, 90% of the trajectory steps are below 0.5 eV lab, and 50% are below 0.1 eV lab.

These trajectory sets were run under conditions corresponding to a kinetic energy of 1.85 eV lab (1.0 eV c.m., $NH_3^+ + ND_3$), but no significant dependence of the energy spread on an increasing kinetic energy was observed. The geometry of the injection optics largely determines the radial energy uncertainty of the ion beam in this instrument. Thus, the uncertainty is somewhat fixed, which demonstrates the importance of careful optics design. Although the accuracy of these simulations is limited by their two-dimensional representation of a three-dimensional geometry, the results are used to indicate roughly how the configuration performs and how much residual radial kinetic energy the ion beam has in the collision region.

The experimental ion beam energy characterizations address only the axial kinetic energy and employ two approaches, each of which determines the ion beam axial kinetic energy offset and spread. Yet both approaches are sufficiently flawed as to require corroboration. The first approach uses the TOF analysis of a chopped ion beam. The second uses the octopole ion-guide dc potential as a retarding field to determine directly the energy profile of the ion beam.

The TOF experiments measure the arrival time of a short (~3 μs) ion pulse at fast (~14 eV lab) and slow (~0.7 eV

lab) octopole voltage settings, which correspond, respectively, to short and long octopole residence times. To minimize distortions, the pulsing setup was initially configured by superimposing the chopping pulse onto NH_3^+ photoions generated with a pulsed nanosecond laser (see the following paper[1]). The unchopped photoions have a pulse width of a few microseconds. The pulsing conditions were adjusted to minimize both the temporal width and shift distortions imposed upon the photoion packet when the pulsing optic was activated. The relative difference between the two arrival times, keeping all other conditions constant, yielded an underlying ion beam kinetic energy of 0.25 eV for the N^+ ions formed by electron impact. The corresponding ion pulse widths are used to extract the kinetic energy spread of the ion pulse. The width of the fast ion pulse is slightly shorter than the generating ion optic chopping pulse. The width of the slow ion pulse is nearly seven times the chopping pulse width. This change in width is used to determine a FWHM kinetic energy spread for both the leading and trailing edges of the ion pulse. The trailing edge energy spread shows a significant distortion that is attributed to the chopping that creates the ion pulse; the observed energy width of the trailing edge half-maximum was 5 times smaller than that of the leading edge. An estimated kinetic energy spread of 0.4 eV is obtained by doubling the half-width energy spread needed to reproduce the larger leading edge shift.

The octopole ion-guide ramping experiments are performed by ramping the dc offset of the ion guide to yield an energy cutoff profile that, when differentiated, is the energy profile of the ion beam. The kinetic energy offset and spread of the ion beam can be read directly from this profile. Ambiguities are introduced into this method by the variable lensing that results from the changing octopole potential. Although the trajectory simulations described showed no significant changes in the energy spread as the ion beam kinetic energy was increased above 1.85 eV, these octopole ramping experiments are expected to have a significant sensitivity to the slight changes in focusing that accompany the scanning octopole potential as the average kinetic energy approaches zero. Typical ion beam kinetic energy offsets observed from these energy profiles were ~0.5 eV. The uncertainties inherent in this method do not affect the relative stability of the measurement, which when combined with the ease of experimental use, was the motivation behind our selection of this method to track the day-to-day kinetic energy magnitude and spread of the ion beam. Reaction data for the present $N^+ + O_2$ study were collected only when the laboratory frame energy uncertainty of the ion beam, as measured by octopole ramping, was below 1.1 eV (0.77 eV c.m.) FWHM but typically not less than 0.8 eV lab.

The ion beam kinetic energy characteristics observed with the TOF analysis are systematically smaller than those observed with the octopole ramping. The kinetic energy offset observed with the TOF analysis was 0.25 eV lab, compared to ~0.5 eV with the octopole ramping. The kinetic energy spread observed with the TOF analysis was 0.4 eV lab, compared to 0.8–1.1 eV with the octopole ramping. Each measurement method is sensitive to uncertainties, and the true energy characteristics likely lie between these values. We have slightly more confidence in the kinetic energy offset measured with the TOF analysis because of the checks we were able to perform and the rigor of the technique. Hence, the 0.25 eV offset was used to correct all the reported collision energies, but the absolute value of the collision energies may be larger as indicated by the octopole ramping measurements. The overall kinetic energy spread is estimated to be in the range of 0.9–1.6 eV lab (0.6–1.1 eV c.m.), which results from summing the radial energy spread (0.5 eV lab) with the TOF analysis and octopole ramping axial uncertainties, respectively.

E. Collision energy spread

The center-of-mass collision energy, neglecting the thermal motion of the neutral reagent, is given by

$$E_{\text{c.m.}} = E_{\text{lab}}\left(\frac{M}{m+M}\right) = 0.70E_{\text{lab}}, \tag{3}$$

where E_{lab} is the kinetic energy of the reagent ion in the lab frame, m is the mass of the reagent ion ($m=14$), and M is the mass of the thermal neutral reagent ($M=32$). Using this formula, the ion beam kinetic energy spread from above, 0.9–1.6 eV lab, corresponds to a center-of-mass collision energy spread of 0.6–1.1 eV c.m.

Because the ion-molecule studies described in this paper are carried out under beam-gas conditions, there can be an additional sizable spread in the collision energy resulting from the thermal motion of the neutral reagents ($E_{\text{av}}=3/2kT=0.039$ eV). This thermal uncertainty may be larger than the uncertainty resulting from the ion beam kinetic energy spread. The thermal motion of the neutral target gas causes the collision energy distribution to have a full width at half maximum of[30]

$$\Delta E_{\text{FWHM}} = \left[11.1\left(\frac{m}{m+M}\right)kTE_{\text{c.m.}}\right]^{1/2} = 0.30(E_{\text{c.m.}})^{1/2}, \tag{4}$$

neglecting any spread in the ion beam energy. At collision energies of 1.0 and 10.0 eV, the ΔE_{FWHM} spreads are 0.3 and 0.9 eV, respectively. Note that this spread is comparable to the width of the kinetic energy distribution of the reagent ions, and at higher collision energies, it may exceed the spread in the kinetic energy of the reagent ions.

III. RESULTS AND DISCUSSION

Figure 4 presents our measured branching ratios for the $N^+ + O_2$ reaction as a function of collision energy. For comparison, the branching ratio results of the crossed beam experiments of Neynaber, Rutherford, and Vroom,[2] the drift tube measurements of Howorka, Dotan, Fehsenfeld, and Albritton,[3] and several thermal energy branching ratio measurements[4–6] are also shown. At the higher collision energies (1.5–10 eV c.m.), the branching ratio trends and magnitudes reported here are in good agreement with the existing results. The ordering of the channel intensities is correctly reproduced over this energy range, although a slight systematic shift independent of collision energy is observable in the branching fractions. Our measured O_2^+ branching ratios are

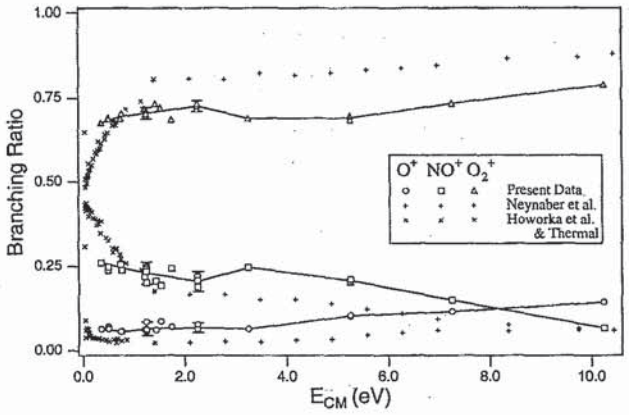

FIG. 4. Product branching ratios for the reaction $N^+ + O_2$ plotted as a function of center-of-mass collision energy ($E_{c.m.}$) comparing the present work with the measurements of Neynaber *et al.* (Ref. 2), Howorka *et al.* (Ref. 3), and several thermal measurements (Refs. 4–6). Error bars are two standard deviations.

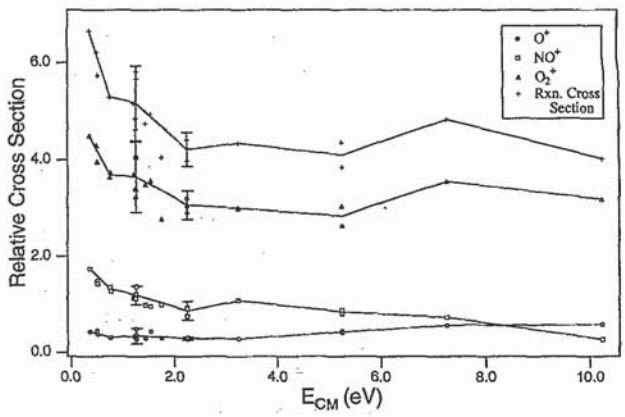

FIG. 5. Product relative cross sections and the total reaction cross section for the reaction $N^+ + O_2$ plotted as a function of center-of-mass collision energy ($E_{c.m.}$). Error bars are two standard deviations.

systematically ~0.15 lower than those observed by Neynaber *et al.*, with a corresponding increase in the branching ratio of the NO^+ and O^+ channels. At lower collision energies (less than 1.5 eV c.m.), our measurements do not reproduce the curvature observed in the drift tube measurements.

For a wide range of collision energies (1.5–10 eV c.m.), the branching ratio comparisons demonstrate our quadrupole-octopole-quadrupole instrument has no significant bias in collecting the product channels of the $N^+ + O_2$ system. The slight discrepancy in the branching ratios is not significantly energy dependent and therefore not strongly indicative of channel-dependent discrimination. Likely it is the result of a systematic error in one or both of the measurement techniques. The nature of the processes leading to formation of the three primary ion products is sufficiently different that the product ions are expected to cover a fairly broad range of kinetic energies, although only the NO^+ product kinetic energy distribution has been measured above thermal collision energies.[31,32] The agreement seen in the high collision energy branching ratios indicates fairly uniform detection efficiency for the three product channels, answering affirmatively the third and remaining question put forth in Sec. I: Can product intensities be measured without significant channel-dependent discrimination? The favorable reproduction by our apparatus of the $N^+ + O_2$ branching ratios for collision energies greater than 1.5 eV c.m. (2 eV lab) provides the basis upon which can be built subsequent presentation and interpretation of product ion intensities from state-selected studies down to collision energies of at least 1.5 eV c.m.

The primary cause of the discrepancy observed below 1.5 eV c.m. is believed to be the kinetic energy spread of the reactant ion beam convoluted with the thermal spread of the neutral reactant, and not a channel-dependent discrimination. Simulated convolutions of model cross sections with an ion beam having an energy width of 0.8 eV c.m. indicate that the low collision energy curvature of the drift tube branching ratios cannot be reproduced, and the resulting convolutions closely reproduce our low collision energy branching ratios. Given the agreement between our measurements and those of Albritton and co-workers above 1.5 eV c.m.,[3] in combination with our experimentally estimated ion beam energy spread of 0.8 eV c.m., we are confident that our measurements above 1.5 eV c.m. (2.1 eV lab) are not significantly affected by the collision energy spread inherent in our configuration.

In Fig. 5 we present the product relative cross sections, corresponding to the branching ratios in Fig. 4, as a function of collision energy. The absolute cross section results of Neynaber *et al.*[2] are presented in Fig. 6 for comparison. Because the determination of a scaling factor to transform our relative cross sections to absolute values has proven difficult, the relative nature of our cross section measurements allows only qualitative comparisons to the data of Neynaber *et al.* The trends observed in each of the cross section measurements agree closely. The minor product channel trends (O^+, NO^+) observed by Neynaber *et al.* are well reproduced by our measurements; the O^+ cross section has a slow, steady

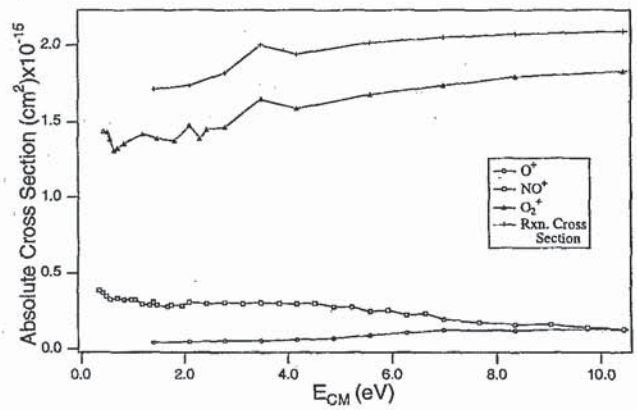

FIG. 6. Product absolute cross sections and the total reaction cross section of the Neynaber *et al.* (Ref. 2) crossed beam experiments for the reaction $N^+ + O_2$ plotted as a function of collision energy ($E_{c.m.}$).

rise as collision energy is increased, and the NO^+ cross section steadily decreases. Both data sets have a crossover of the two minor channel cross sections between 8 and 10 eV c.m. The O_2^+ cross sections are more difficult and less favorable to compare. The trend in the data of Neynaber *et al.* is toward higher cross sections with increasing collision energy, whereas our O_2^+ cross sections show a different dependence on collision energy. Up to 5 eV c.m., the cross section decreases with increasing collision energy, paralleling the decrease observed in NO^+. Above 5 eV c.m., a slight rise in the O_2^+ cross section with collision energy may be detectable. This discrepancy in the O_2^+ cross sections may indicate that it is the channel responsible for the systematic shifts in the branching ratio measurements discussed above. Without an objective way to scale our relative cross sections to absolute values, no real comparison of cross section magnitudes can be made.

IV. CONCLUSIONS

This paper addressed two questions regarding the experimental performance of our quadrupole-octopole-quadrupole instrument in studying ion-molecule reactions: (1) Can the collision energy be accurately controlled and can the spread be narrow enough to yield meaningful collision energies? (2) Can product intensities be measured without significant channel-dependent discrimination? The ion beam energy characteristics outlined in Sec. II yield a kinetic energy width of less than 1.6 eV lab (1.1 eV c.m.) and a kinetic energy offset of ~0.25 eV lab. For the collision energies to be investigated with this instrument (1–20 eV lab), this energy width and offset are sufficiently small to yield meaningful collision energies. With the good agreement between our measured branching ratios for the $N^+ + O_2$ system and the measurements of both Neynaber *et al.*[2] and Albritton and co-workers,[3] we are confident that our measured product intensities are not subject to significant channel-dependent discrimination above collision energies of at least 1.5 eV c.m. (2.1 eV lab), i.e., interpretation of the product ion intensity variations measured with this instrument is valid above 1.5 eV c.m.

ACKNOWLEDGMENTS

This work was supported by the Air Force Office of Scientific Research under Grant No. AFOSR-89-0264 and AFOSR-F49620-92-0074. L.A.P. was supported by a National Science Foundation Postdoctoral Research Fellowship in Chemistry (CHE-8907493). B.A.K. received partial support from the Swiss National Science Foundation.

[1] L. A. Posey, R. D. Guettler, N. J. Kirchner, and R. N. Zare, J. Chem. Phys. **101**, 3772 (1994), following paper.
[2] R. H. Neynaber, J. A. Rutherford, and D. A. Vroom, Gulf Radiation Technology Report No. Gulf-RT-A12209 (DNA 2944F), July, 1972.
[3] F. Howorka, I. Dotan, F. C. Fehsenfeld, and D. L. Albritton, J. Chem. Phys. **73**, 758 (1980).
[4] J. L. McCrumb and P. Warneck, J. Chem. Phys. **66**, 5416 (1977).
[5] D. Smith, N. G. Adams, and T. M. Miller, J. Chem. Phys. **69**, 308 (1978).
[6] V. G. Anicich, W. T. Huntress, Jr., and J. H. Futrell, Chem. Phys. Lett. **47**, 488 (1977).
[7] J. W. Farley, Rev. Sci. Instrum. **56**, 1834 (1985).
[8] B. A. Huber, T. M. Miller, P. C. Cosby, H. D. Zeman, R. L. Leon, J. T. Moseley, and J. R. Peterson, Rev. Sci. Instrum. **48**, 1306 (1977).
[9] H. D. Zeman, Rev. Sci. Instrum. **48**, 1079 (1977).
[10] K. M. Ervin, Ph.D. thesis, University of California, Berkeley, 1986.
[11] R. J. S. Morrison, W. E. Conaway, and R. N. Zare, Chem. Phys. Lett. **113**, 435 (1985).
[12] R. J. S. Morrison, W. E. Conaway, T. Ebata, and R. N. Zare, J. Chem. Phys. **84**, 5527 (1986).
[13] W. E. Conaway, T. Ebata, and R. N. Zare, J. Chem. Phys. **87**, 3453 (1987).
[14] W. E. Conaway, T. Ebata, and R. N. Zare, J. Chem. Phys. **87**, 3447 (1987).
[15] T. Ebata and R. N. Zare, Chem. Phys. Lett. **130**, 467 (1986).
[16] K. M. Ervin and P. B. Armentrout, J. Chem. Phys. **83**, 166 (1985).
[17] D. Gerlich, in *State-Selected and State-to-State Ion-Molecule Reaction Dynamics, Part I: Experiment*, edited by C.-Y. Ng and M. Baer (Wiley, New York, 1992), p. 1.
[18] M. H. Friedman, A. L. Yergey, and J. E. Campana, J. Phys. E **15**, 53 (1982).
[19] N. G. Adams, D. Smith, and J. F. Paulson, J. Chem. Phys. **72**, 288 (1980).
[20] W. T. Huntress, Jr., M. M. Mosesman, and D. D. Elleman, J. Chem. Phys. **54**, 843 (1971).
[21] R. S. Hemsworth, J. D. Payzant, H. I. Schiff, and D. K. Bohme, Chem. Phys. Lett. **26**, 417 (1974).
[22] T. Baer and P. T. Murray, J. Chem. Phys. **75**, 4477 (1981).
[23] R. D. Guettler (unpublished).
[24] S. Scherbath and D. Gerlich, J. Chem. Phys. **90**, 1610 (1989).
[25] MacSimion, vers. 2.0 (Montech Pty. Ltd., Victoria, Australia, 1991), Computer: Apple Macintosh IIci.
[26] B. E. Evans and R. W. Supple, J. Vac. Sci. Technol. **8**, 270 (1971).
[27] P. H. Dawson, Int. J. Mass Spectrom. Ion Phys. **20**, 237 (1976).
[28] J. E. Campana and P. C. Jurs, Int. J. Mass Spectrom. Ion Phys. **33**, 119 (1980).
[29] J. E. Campana, Int. J. Mass Spectrom. Ion Phys. **33**, 101 (1980).
[30] P. J. Chantry, J. Chem. Phys. **55**, 2746 (1971).
[31] D. Gerlich and M. Wirth, Contributions of the Symposium Atomic Surface Physics, edited by F. Howorka, W. Lindinger, and T. D. Maerk (University of Innsbruck, Innsbruck, Austria, 1986), p. 366.
[32] J. C. Tully, Z. Herman, and R. Wolfgang, J. Chem. Phys. **54**, 1730 (1971).